ACS APPLIED MATERIALS & INTERFACES

Research Article

www.acsami.org

# Contact Resistivity Decrease at a Metal/Semiconductor Interface by a Solid-to-Liquid Phase Transitional Metallo-organic Silver

Dong-Youn Shin,*[,†] Jun-Young Seo,[†] Min Gu Kang,*[,‡] and Hee-eun Song[‡]

[†]Department of Graphic Arts Information Engineering, Pukyong National University, 365, Sinseon-ro, Nam-gu, Busan, 608-739, Republic of Korea

[‡]Solar Energy Research Centre, Korea Institute of Energy Research, Daejeon, 305-343, Republic of Korea

**ABSTRACT:** We present a new approach to ensure the low contact resistivity of a silver paste at a metal/semiconductor interface over a broad range of peak firing temperatures by using a solid-to-liquid phase transitional metallo-organic silver, that is, silver neodecanoate. Silver nanoclusters, thermally derived from silver neodecanoate, are readily dissolved into the melt of metal oxide glass frit even at low temperatures, at which point the molten metal oxide glass frit lacks the dissociation capability of bulk silver into $Ag^+$ ions. In the presence of $O^{2-}$ ions in the melt of metal oxide glass frit, the redox reaction from $Ag^+$ to $Ag^0$ augments the noble-metal-assisted etching capability to remove the passivation layer of silicon nitride. Moreover, during the cooling stage, the nucleated silver atoms enrich the content of silver nanocolloids in the solidified metal oxide glass layer. The resulting contact resistivity of silver paste with silver neodecanoate at the metal/semiconductor interface thus remains low—between 4.12 and 16.08 mΩ $cm^2$—whereas without silver neodecanoate, the paste exhibits a contact resistivity between 2.61 and 72.38 mΩ $cm^2$ in the range of peak firing temperatures from 750 to 810 °C. The advantage of using silver neodecanoate in silver paste becomes evident in that contact resistivity remains low over the broad range of peak firing temperatures, thus providing greater flexibility with respect to the firing temperature required in silicon solar cell applications.

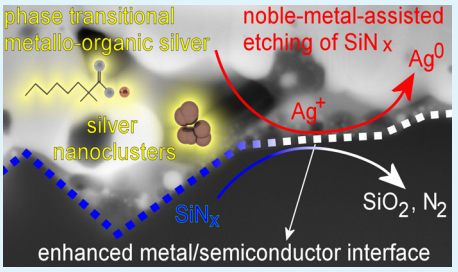


**KEYWORDS:** *metallo-organic silver, phase transition, noble-metal-assisted etching, silver nanocolloids, contact resistivity, silicon solar cell*

## 1. INTRODUCTION

Crystalline silicon solar cells prevail in the market because they offer advantages such as a low manufacturing cost, excellent environmental stability, and high cell efficiency.[1,2] As the industrial demand for higher cell efficiency using a thinner silicon solar cell wafer rapidly increases, various noncontact metallization techniques for the construction of finer silver electrodes to reduce shading loss have been demonstrated, such as aerosol jet printing,[3,4] dispensing printing,[5] inkjet printing,[6,7] and electrohydrodynamic jet printing.[8] However, the construction of finer silver electrodes does not inevitably improve cell efficiency because the contact resistivity increases.[9] Therefore, to retain low contact resistivity with finer silver electrodes, the formation of nickel silicide (NiSi) has been proposed.[10,11] However, this approach for the formation of NiSi at the interface between silver electrodes and the emitter layer of a silicon solar cell is not only vulnerable to nickel oxidation, particularly when the deposited nickel layer is annealed in the ambient environment, but also susceptible to the annealing temperature, which is approximately 420 °C. At temperatures either below or above 420 °C, a different type of a nickel silicide alloy, such as nickel disilicide ($NiSi_2$) or dinickel silicide ($Ni_2Si$), thereby increases contact resistivity.[12] It should be noted that the maximization of cell efficiency depends not only on the formation of a sound contact between silver electrodes and the emitter layer on the front side of a silicon solar cell but also on the optimal formation of the back surface field, which is prepared using aluminum paste, on the backside. Because aluminum particles must melt and react with silicon to form a thin layer of aluminum−silicon alloy, the required firing temperature should be higher than the aluminum and silicon eutectic temperature of 577 °C.[13] Consequently, the firing temperature range for the formation of NiSi becomes incompatible with that for the formation of aluminum−silicon alloy on the backside of a silicon solar cell.

To achieve compatibility with the conventional firing temperature range, researchers and developers have explored the combinatorial use of additives in silver paste, such as silver acetate ($CH_3COOAg$) with aluminum metallic glass frit,[14] or quaternary phosphonium salts with metal oxide glass frit.[15] In the former case, silver acetate functions as a diffusion barrier for aluminum in the metallic glass frit, which adversely acts as a p-type dopant to the n-type emitter layer, thereby enabling the fabrication of interdigitated back-contact silicon solar cells. Although the resulting cell efficiency is as high as 20.3%, this approach has limited applicability, particularly when a conventional silicon solar cell with a silicon nitride ($SiN_x$) layer formed on its top surface is considered. Because aluminum metallic

**Received:** June 5, 2014
**Accepted:** September 3, 2014
**Published:** September 3, 2014

 © 2014 American Chemical Society 

glass frit lacks the ability to etch the $SiN_x$ layer, as metallic oxide glass frit does through a redox reaction,[16] it can be used for only limited types of silicon solar cells with no $SiN_x$ layer formed at the contact. Moreover, silver acetate has little solubility in the nonpolar organic solvents commonly used in silver pastes, such as $\alpha$-terpineol; hence, the choice of organic solvent might be substantially restrained for the formulation of homogeneous silver paste.

Another approach to lowering contact resistivity through the combinatorial use of a phosphorus-containing chemical compound with metal oxide glass frit is more useful in this respect. The phosphorus-containing chemical compound acts as a dispersant as well as an n-type dopant. Therefore, it can be dissolved in the wide range of organic solvents and undergo self-doping into the existing n-type emitter layer of a silicon solar cell. However, this approach is difficult to apply to silicon solar cells with high emitter sheet resistance because the high thermal budget at approximately 870 °C for the effective self-doping of a phosphorus-containing chemical compound is likely to adversely affect the lightly doped n-type emitter layer.

Therefore, a more facile additive that can be readily dissolved in commonly used nonpolar organic solvents and that exhibits low contact resistivity over the broad range of peak firing temperatures is needed. In this study, a solid-to-liquid transitional metallo-organic silver, that is, silver neodecanoate ($C_{10}H_{19}AgO_2$), is proposed as a new combinatorial additive with metal oxide glass frit, and the underlying mechanism of silver neodecanoate's contribution to low contact resistivity over a broad range of peak firing temperatures is investigated.

## 2. EXPERIMENTAL SECTION

**2.1. Materials.** The primary components of the in-house developed silver paste were silver particles (HP-0710, D50 = 0.9−1.4 $\mu$m, Heesung Metal, Ltd., Seoul, Republic of Korea) and metal oxide glass frit (V2172, $SiO_2$−PbO−ZnO, D50 ≈ 2.58 $\mu$m, Ceradyne, Inc., Seattle, WA, USA). For the homogeneous dispersion of silver particles and metal oxide glass frit in a carrier vehicle ($\alpha$-terpineol, CAS No. 98-55-5, Kanto Chemical Co., Inc., Tokyo, Japan), a polymeric dispersant (Zephrym PD 2246 SF, Croda International, Plc., Snaith, UK) was added. Ethyl cellulose (CAS No. 9004-57-3, Sigma-Aldrich, St. Louis, MO, USA) was used to aid the dispersion of silver particles and metal oxide glass frit and to prevent cracking of the dried silver electrodes. As a solid-to-liquid phase transitional metallo-organic silver, silver neodecanoate (CXSV060, Gelest, Inc., Philadelphia, PA, USA), which readily dissolves in $\alpha$-terpineol, was chosen.

Two types of silver paste were formulated. The first type of silver paste consisted of 80 wt % solid content of silver particles and metal oxide glass frit at a weight ratio of 93:7, and 2.5 wt % of silver neodecanoate with respect to the silver particles and metal oxide glass frit. The second type of silver paste consisted of 90 wt % solid content of silver particles and metal oxide glass frit at a weight ratio of 89:11, and 5 wt % of silver neodecanoate with respect to the silver particles and metal oxide glass frit.

The emitter sheet resistance of monocrystalline silicon wafers with a topmost layer of $SiN_x$ was approximately 50 Ω/sq (KPE Co., Republic of Korea) and 77 Ω/sq (Shinsung Solar Energy Corp., Republic of Korea). After the silver paste was screen-printed, silicon wafers were dried on a hot plate stirrer at 150 °C for 2 min and were then fired using a rapid thermal processor (AccuThermo AW 610, Allwin21 Corp., USA). From the commencement of the firing process, dry air was fed at a flow rate of 5 L/min. The first ramp from room temperature to 300 °C required 4 s. After the second drying period at 300 °C for 20 s, the temperature was increased to 400 °C within 6 s and then to 500 °C within 8 s to facilitate the thermal decomposition of organic species in the silver paste during the burnout period. Finally, the peak firing temperature was attained within 4.6 s, and the sample was then cooled by natural convention. The experimented peak firing temperatures for the measurement of the contact resistivity of silver paste with or without silver neodecanoate was in the range of 750−830 °C.

**2.2. Characterization.** The viscosity of the silver paste was measured using a rheometer (RheoScope 1, Thermo Fisher Scientific, Inc., Germany). To calculate contact resistivity by using a three-point probe method,[17−19] resistance measurements between discrete silver electrodes at the spacing of 2 mm were conducted using a probe station (MST 4000A, MS Tech Co., Ltd., Republic of Korea) and a source meter (Model 2401, Keithley Instruments, Inc., USA). The line width of the silver electrodes was measured with an optical microscope (JSZ-7XT, Samwon Scientific Ind. Co., Ltd., Republic of Korea). A field-emission transmission electron microscope (Tecnai $G^2$ F30 S-Twin, FEI Corp., USA) was used to perform transmission electron microscopy (TEM), elemental mapping, and selective-area electron diffraction (SAED), and the microscopic images were captured with a field-emission scanning electron microscope (SUPRA-55VP, Carl Zeiss NTS GmbH, Germany) for morphological analysis. The thermogravimetric analysis (TGA) and differential scanning calorimetric (DSC) analysis were conducted using a thermal analyzer (Setsys 16/18, SETARAM Instrumentation, France). Crystalline materials were identified by X-ray diffraction (XRD) (X'Pert-MPD System, Koninklijke Philips N.V., The Netherlands).

## 3. RESULTS AND DISCUSSION

**3.1. Impact of Silver Neodecanoate on the Rheological Characteristics of Silver Paste.** Silver neodecanoate offers several advantages when used in silver paste. One such advantage is its ability to decrease the electrical resistivity of silver electrodes, as it eventually turns into a highly conductive metallic state when thermally decomposed.[20,21] Because silver nanoclusters produced through the thermal decomposition of silver neodecanoate bridge the silver particles in the silver paste, the decrease of electrical resistivity becomes evident, particularly when the firing temperature is low.[22,23] Another advantage of using silver neodecanoate in silver paste is that it reduced viscosity from 3.3 to 2.3 kcP at a solid content of 80 wt % and from 213.5 to 116.7 kcP at a solid content of 90 wt % when the shear strain rate and temperature were set to 10 $s^{-1}$ and 23 °C, respectively, as shown in Figure 1. This decrease in viscosity results from the silver neodecanoate's molecular structure and excellent solubility in $\alpha$-terpineol, unlike silver acetate. Silver neodecanoate's molecular structure resembles that of commonly used carboxylic acid-based dispersants, such as caprylic acid ($CH_3(CH_2)_6COOH$), lauric acid ($CH_3(CH_2)_{10}COOH$), or oleic acid ($CH_3(CH_2)_7CH{=}CH(CH_2)_7COOH$), with the exception that the hydrogen atom of its carboxylic group is substituted with a silver atom through ionic bonding.[24] After it dissolves in $\alpha$-terpineol, the silver neodecanoate behaves analogously to a capping agent when its silver atom is adsorbed onto the surface of a silver particle where a polymeric dispersant is not anchored.[25] In contrast, silver acetate cannot be added to such silver paste with the solid

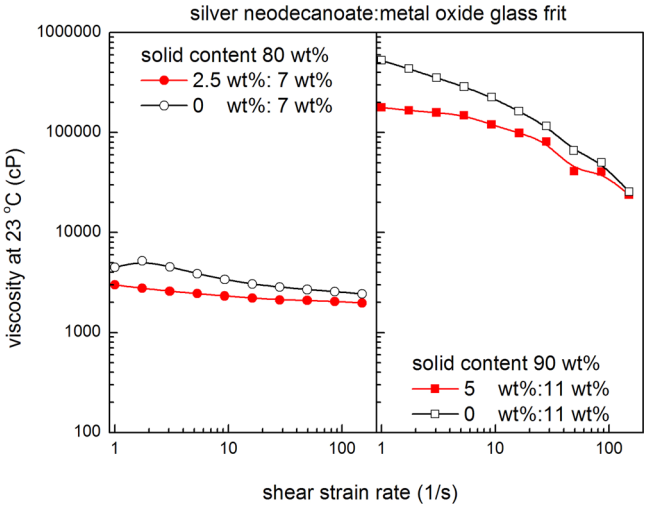


**Figure 1.** Viscosity of silver paste with and without silver neodecanoate.

content as high as 90 wt % because it is insoluble in $\alpha$-terpineol. Consequently, silver acetate does not contribute to the viscosity decrease of silver paste at all.

**3.2. Impact of Silver Neodecanoate on the Contact Resistivity of Silver Paste.** Figure 2 shows that the contact

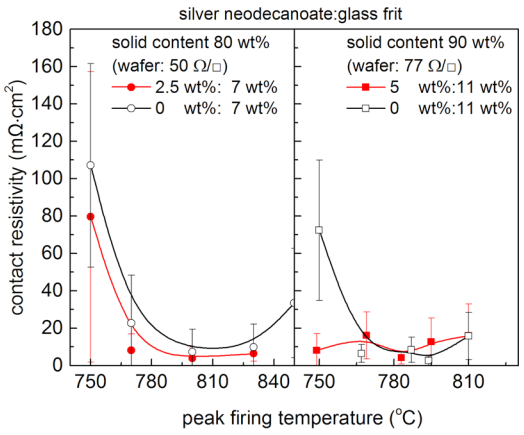


**Figure 2.** Influence of silver neodecanoate on the contact resistivity at different peak firing temperatures.

resistivity of silver paste without silver neodecanoate generally exhibited a parabolic behavior at peak firing temperatures from 750 to 830 °C. If the peak firing temperature is too high, then a thick metal oxide glass layer tends to form at the metal/semiconductor interface, and the contact resistivity gradually increases. If the peak firing temperature is too low, however, the metal oxide glass frit has insufficient chemical activity to etch the $SiN_x$ layer via a redox reaction[16] and the contact resistivity dramatically increases. In contrast, silver paste with silver neodecanoate maintained a contact resistivity lower than that of silver paste without silver neodecanoate. This phenomenon became pronounced when the content of silver neodecanoate with respect to the silver particles and metal oxide glass frit was increased from 2.5 to 5 wt % at a low peak firing temperature of 750 °C.

Silver nanoclusters are known to form silver silicate ($Ag_2SiO_3$) on a silicon oxide surface under oxidizing conditions,[26] or metastable amorphous silver silicide through the diffusion of silver atoms from silver nanoclusters into the amorphous silicon at approximately 700 °C.[27] Similarly, silver nanoclusters from silver neodecanoate can be postulated to form a conductive alloy, which might be responsible for the low contact resistivity, even though the $SiN_x$ layer was not fully etched away at such a low peak firing temperature as 750 °C. To investigate this hypothesis, we spin-coated a 25 wt % solution of silver neodecanoate in xylene onto a $SiN_x$-coated monocrystalline silicon wafer and fired it at approximately 800 °C. For purposes of comparison, another sample coated with silver particles was also prepared.

As shown in Figure 3, a polycrystalline silver structure was observed on top of the $SiN_x$ layer when silver particles were fired. In contrast, a thin layer with a single-crystalline silver structure was observed on top of the $SiN_x$ layer when silver neodecanoate was fired. However, there was no evidence that silver atoms either diffused into or formed an alloy with the underlying $SiN_x$ layer. In fact, the $SiN_x$ layer remained intact in both cases. This observation supports the fact that the contact resistivity of silver paste with and without silver neodecanoate was statistically equal within a 5% level of significance, 694.48 ± 159.60 and 648.13 ± 197.64 mΩ $cm^2$, respectively, when metal oxide glass frit was completely removed from the silver paste. This observation also indicates that silver neodecanoate alone cannot react with the $SiN_x$ layer.

A notable result in Figure 3 is that the case with silver neodecanoate left substantially fewer voids between the silver and $SiN_x$ layers. To further investigate this phenomenon, silver paste with and without silver neodecanoate was screen-printed onto a textured silicon wafer and fired. The microscopic cross-sectional images of both cases are presented in Figure 4. As with Figure 3, fewer voids were observed, even at steep furrows of the textured surface of a silicon wafer in the case of silver paste with silver neodecanoate. The fraction of voids at the interface was quantitatively analyzed with 90 wt % silver paste at 750 °C on planar silicon wafers. After cropping SEM images at the interface, those images were converted to black and white, and then black pixels which correspond to voids were counted. Without silver neodecanoate, the fraction of voids at the interface was 49.3%. In contrast, the fraction of voids at the interface with 5 wt % of silver neodecanoate decreased to 17.3%. Therefore, we tentatively concluded that silver paste with silver neodecanoate resulted in better interfacial contact formation between silver electrodes and the emitter layer on the textured surface of a silicon wafer, compared to that of silver paste without silver neodecanoate.

This enhanced interfacial contact of silver paste with silver neodecanoate appears to be attributable primarily to the latter's low viscosity. Another reason for the enhanced interfacial contact might be the silver neodecanoate's thermal characteristics. As shown in Figure 5, TGA and DSC thermograms of isomers of silver neodecanoate, that is, silver 2,5-dimethyl-2-ethylhexanoate, silver 2,2-dimethyloctanoate, and silver 2,2-diethylhexanoate, show endothermic peaks in the temperature range of 108−183 °C prior to their thermal decomposition in the temperature range of 196−257 °C. These endothermic peaks indicate that these isomers undergo a solid-to-liquid phase transition prior to their thermal decomposition; thus, the melt of silver neodecanoate could wet the $SiN_x$ layer to minimize the occurrence of voids. In this respect, silver neodecanoate differs from silver acetate because silver acetate does not undergo this solid-to-liquid phase transition prior to its thermal decomposition.[28] Notably, the organic binder used

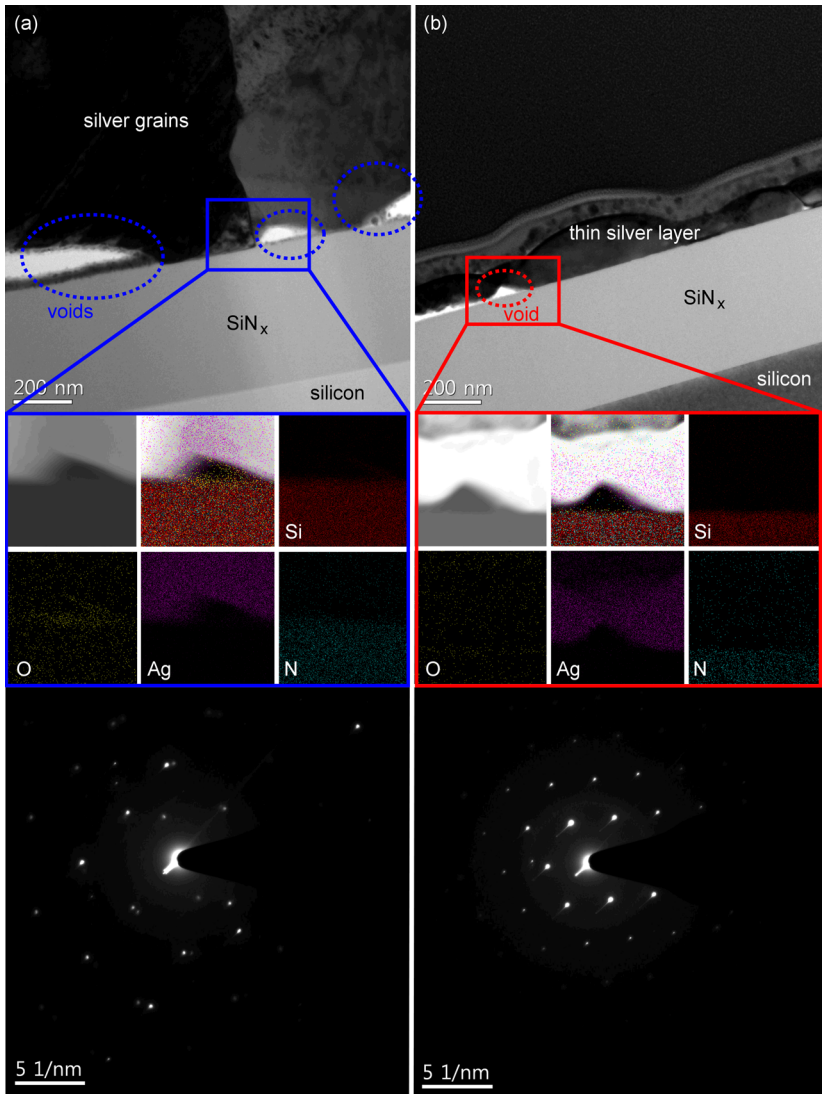


**Figure 3.** TEM, element maps, and SAED images of (a) fired silver particles and (b) fired silver neodecanoate on $SiN_x$-coated monocrystalline silicon wafers.

in silver paste, that is, ethyl cellulose, is vividly decomposed at approximately 345 °C, as shown in Figure 6. Therefore, ethyl cellulose must remain, even after the silver neodecanoate has been fully converted to silver nanoclusters.

To investigate the interaction between silver neodecanoate and ethyl cellulose at different thermal decomposition temperatures, both were dissolved in the carrier vehicle at a weight ratio of 2.5:1 and were subsequently spin-coated onto small square pieces of textured silicon wafers. The first sample was dried at 80 °C for 1 h and left in a vacuum desiccator for 1 day to remove any remnant solvent. The second sample was dried at 80 and 150 °C for 10 min and at 200 °C for 30 min to remove any remnant solvent. The third sample was dried at 80, 150, and 200 °C for 10 min and then subjected to a rapid thermal annealing until 500 °C. The final sample was dried at 80, 150, and 200 °C for 10 min and then subjected to a rapid thermal annealing until 800 °C. The resulting SEM micrographs and XRD patterns of these samples are presented in Figure 7.

By integrating the thermal characteristics of silver neodecanoate and ethyl cellulose with experimental observations, we developed a new hypothesis, as follows. When silver paste with silver neodecanoate is dried, silver neodecanoate and ethyl cellulose coexist in a solid phase, as shown in Figure 7a. However, when the firing temperature reaches the solid-to-liquid phase transition temperature of silver neodecanoate, the melt of silver neodecanoate begins to seep from the mixture of silver neodecanoate and ethyl cellulose and wets the voids between the silver electrodes and the emitter layer on the textured surface of a silicon wafer. As the firing temperature eventually exceeds the thermal decomposition temperature of silver neodecanoate of 196 °C, silver nanoclusters begin to be produced, as shown in Figure 7b; however, ethyl cellulose remains and surrounds the silver nanoclusters. If the firing temperature is greater than 345 °C, ethyl cellulose burns away and the surface of the silicon wafer becomes covered with a layer of silver nanoclusters, as shown in Figure 7c. Because the formed silver layer preferentially lies at the furrows of silicon pyramids at higher firing temperatures, the top of the silicon pyramids could be exposed, as observed in Figure 7d.

Notably, the top surface of the silicon pyramids is covered generously with silver nanoclusters, as is evident in Figure 8b, where the SEM micrograph was captured using an angle-selective backscattered electron detector. The measured contact

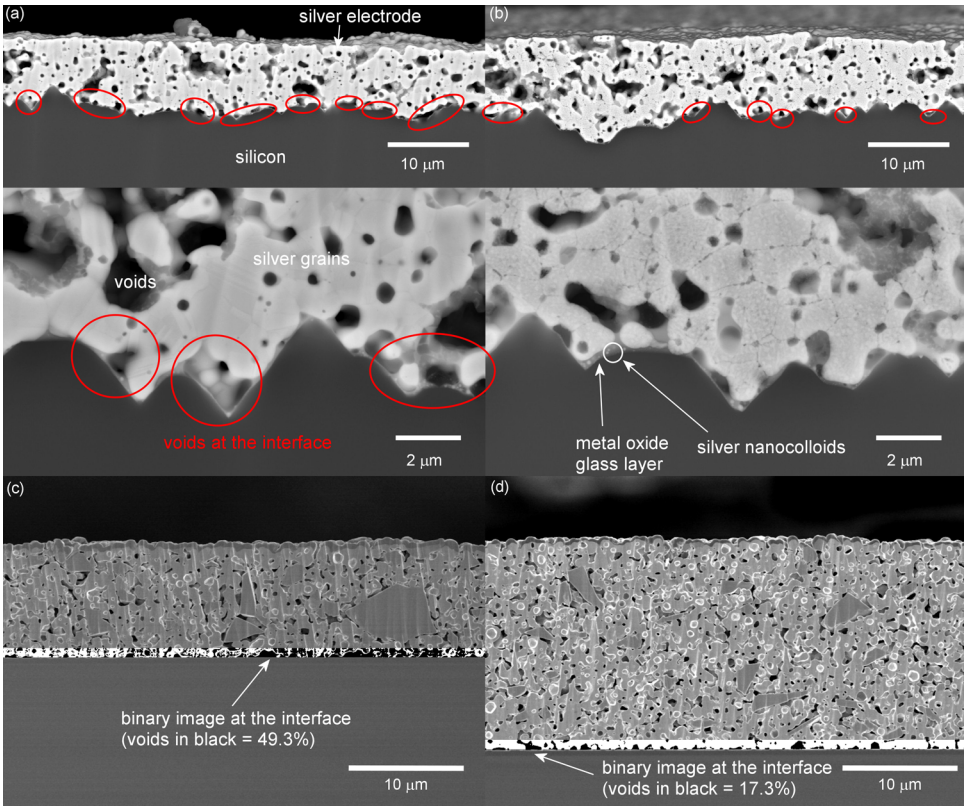


**Figure 4.** Comparison of the interfacial contact of 80 wt % silver paste on textured silicon wafers: (a) without silver neodecanoate (22.68 ± 25.61 mΩ cm$^2$ at 770 °C) and (b) with 2.5 wt % of silver neodecanoate (8.12 + 8.67 mΩ cm$^2$ at 770 °C). Another comparison of the image processed void fraction of 90 wt % silver paste on planar silicon wafers at 750 °C: (c) without silver neodecanoate and (d) with 5 wt % of silver neodecanoate.

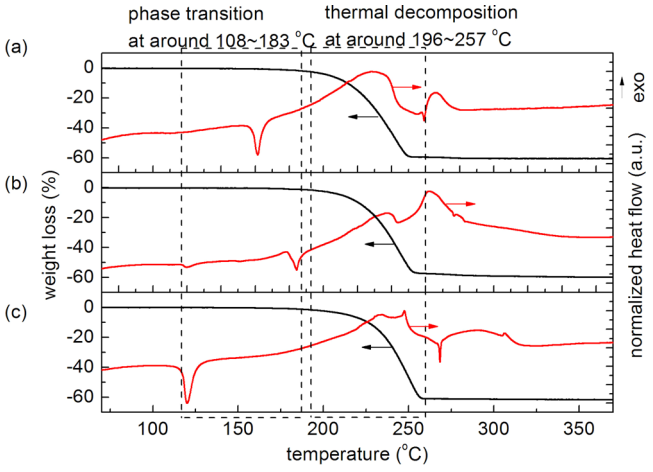


**Figure 5.** TGA and DSC thermograms of isomers of silver neodecanoate: (a) silver 2,5-dimethyl-2-ethylhexanoate, (b) silver 2,2-dimethyloctanoate, and (c) silver 2,2-diethylhexanoate.

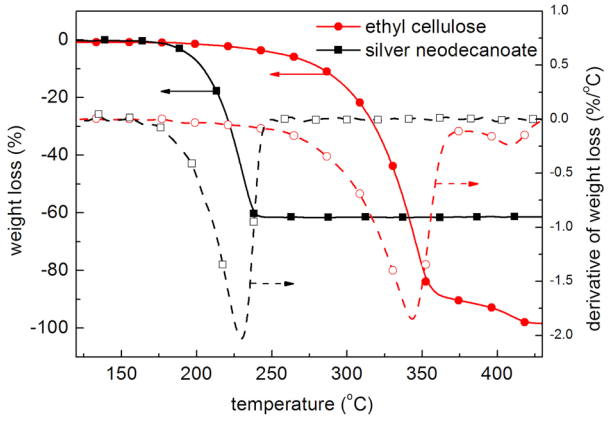


**Figure 6.** TGA thermograms of silver neodecanoate and ethyl cellulose.

resistivity of silver paste, even without metal oxide glass frit, was not infinite, but finite, which implies that the surface passivation of the $SiN_x$ layer is not immaculate, but defective; thus, the emitter layer might be occasionally exposed. Because the top surface of silicon pyramids is likely to be free of a metal oxide glass frit layer,[29] silver nanoclusters formed on the top surface of silicon pyramids, where the $SiN_x$ layer is defective or partially etched away by the metal oxide glass frit at low peak firing temperatures, could serve as electron pickup points and hence help to decrease contact resistivity, although silver neodecanoate alone has no direct capability to either etch or penetrate the $SiN_x$ layer.

### 3.3. Noble-Metal-Assisted Etching of the $SiN_x$ Layer.

Nonetheless, the formed silver nanoclusters on the occasionally defective $SiN_x$ layer cannot be the primary reason why the contact resistivity of silver paste with silver neodecanoate consistently remained low at such a low peak firing temperature of 750 °C, given that the content of silver neodecanoate was 5 wt %. The most plausible explanation for the low contact resistivity achieved at a low peak firing temperature is the noble-metal-assisted etching of the $SiN_x$ layer, as shown in Figure 9. $Ag^+$ ions have been reported to be the major species responsible for etching away the $SiN_x$ layer in the presence of

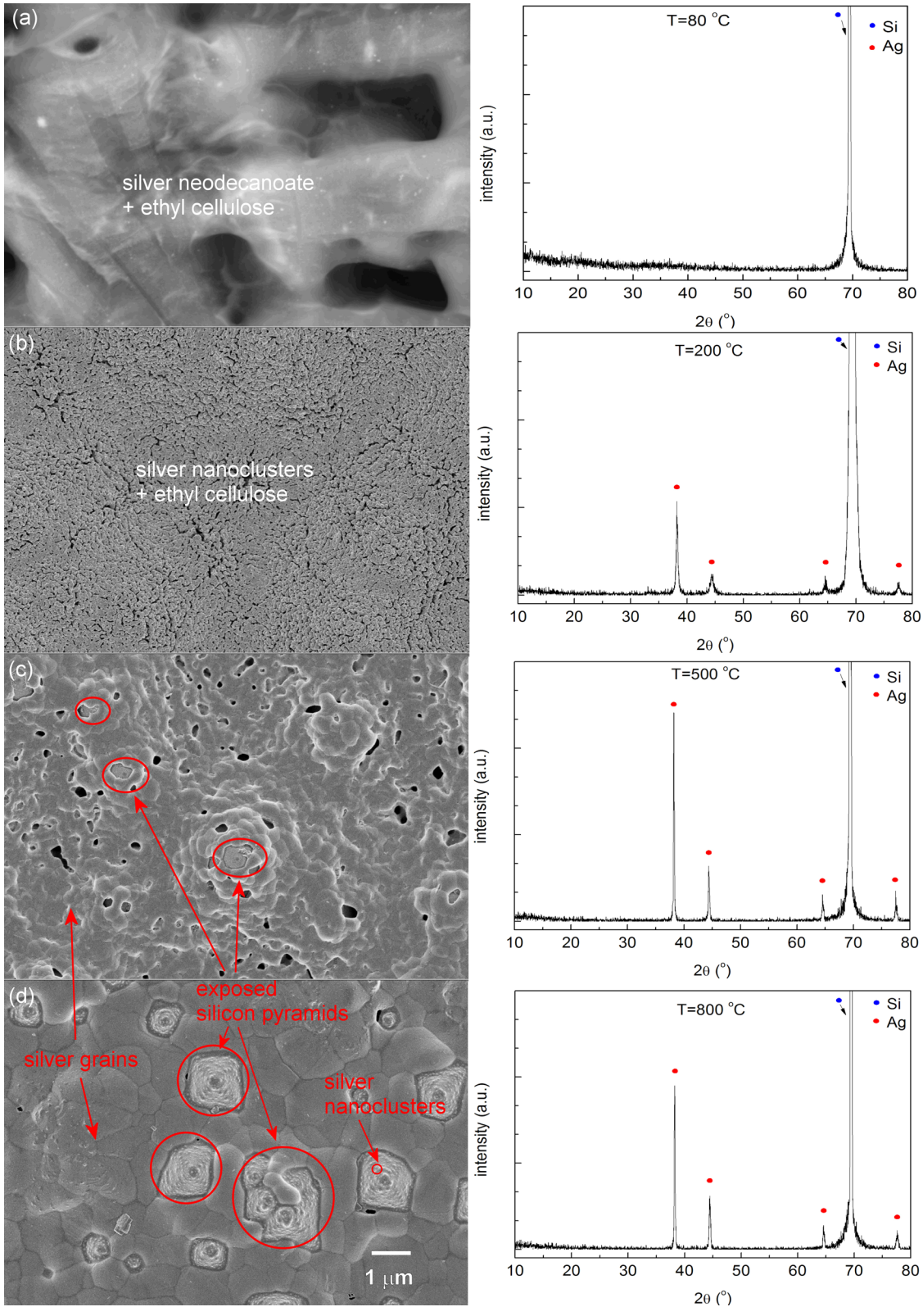


**Figure 7.** SEM and XRD images of the mixture of silver neodecanoate and ethyl cellulose at peak firing temperatures of (a) 80 °C, (b) 200 °C, (c) 500 °C, and (d) 800 °C.

$O^{2-}$ ions via a redox reaction in the melt of metal oxide glass frit,[30−33] which substantially resembles the noble-metal-assisted etching of silicon.[34−38] Because silver nanoclusters from the silver neodecanoate are more readily dissolved into the melt of metal oxide glass frit as $Ag^+$ ions via reaction 1,[33] even at a low peak firing temperature, compared to large silver particles, they could assist the etching of the $SiN_x$ layer, along with $O^{2-}$ ions, through the redox process represented in reaction 2.[33] Abundant $Ag^+$ ions from silver nanoclusters are eventually reduced to $Ag^0$ and are nucleated during the cooling stage. The

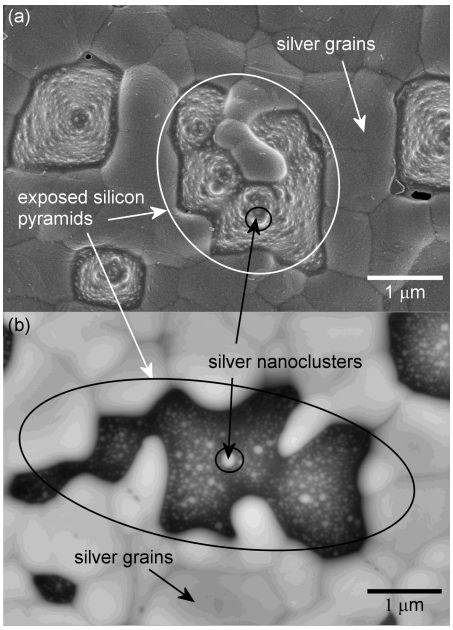


**Figure 8.** SEM images observed with (a) an in-lens secondary electron detector and (b) an angle-selective backscattered electron detector; in both cases, the mixture of silver neodecanoate and ethyl cellulose were fired at 800 °C on a textured silicon wafer.

trace of this process was observed as enriched silver nanocolloids in the solidified metal oxide glass layer, as shown in Figure 10b. These silver nanocolloids can also help to decrease the contact resistivity by assisting electron hopping from the emitter layer to silver electrodes.[39] However, at a sufficiently high peak firing temperature, the contribution of silver neodecanoate to the contact resistivity becomes partially compromised because metal oxide glass frit becomes active enough to dissolve silver particles and provide sufficient $Ag^+$ and $O^{2-}$ ions to etch the $SiN_x$ layer. This mechanism explains why the decrease of contact resistivity with silver neodecanoate at a high peak firing temperature is not as prominent as that at a low peak firing temperature, as shown in Figure 2.

$$4Ag_{(s)} + O_{2(g)} \rightarrow (4Ag^+ + 2O^{2-})_{(\text{in the melt of glass frit})} \quad (1)$$

$$SiN_{x(s)} + (4Ag^+ + 2O^{2-})_{(\text{in the melt of glass frit})} \rightarrow x/2N_{2(g)} + (SiO_2 + 4Ag^0)_{(\text{in the melt of glass frit})} \quad (2)$$

## 4. CONCLUSION

In this study, we investigate how a solid-to-liquid phase transitional metallo-organic silver, that is, silver neodecanoate, influences contact resistivity over a broad range of peak firing temperatures. When the phase of silver neodecanoate changes to liquid at a moderately elevated temperature, the melt of silver neodecanoate seeps from the mixture with ethyl cellulose and eventually fills the voids between silver electrodes and the emitter layer on the textured surface of a silicon wafer. After its thermal decomposition in the temperature range of 196−257 °C, the silver neodecanoate is converted into silver nanoclusters. When metal oxide glass frit melts, silver nanoclusters are readily dissolved into the melt of metal oxide glass frit and become $Ag^+$ ions in the presence of $O_2$. Because $Ag^+$ ions are much nobler than $Pb^{2+}$ ions from the used metal oxide glass frit, they readily participate in the redox reaction to etch the $SiN_x$ layer at a temperature at which $Pb^{2+}$ ions from metal oxide glass frit are not still active enough to initiate the redox reaction. The reduction of silver atoms also contributes to contact resistivity decrease by leaving rich silver nanocolloids in the solidified metal oxide glass layer. Consequently, low contact resistivity can be ensured even at a temperature at which conventional silver paste exhibits high contact resistivity. The resulting contact resistivity of silver paste with silver neodecanoate is between 4.12 and 16.08 mΩ $cm^2$ in the range of peak firing temperatures from 750 to 810 °C. Because the combinatorial use of solid-to-liquid phase transitional silver neodecanoate with metal oxide glass frit is not only facile but also compatible with the conventional firing temperature window for silicon

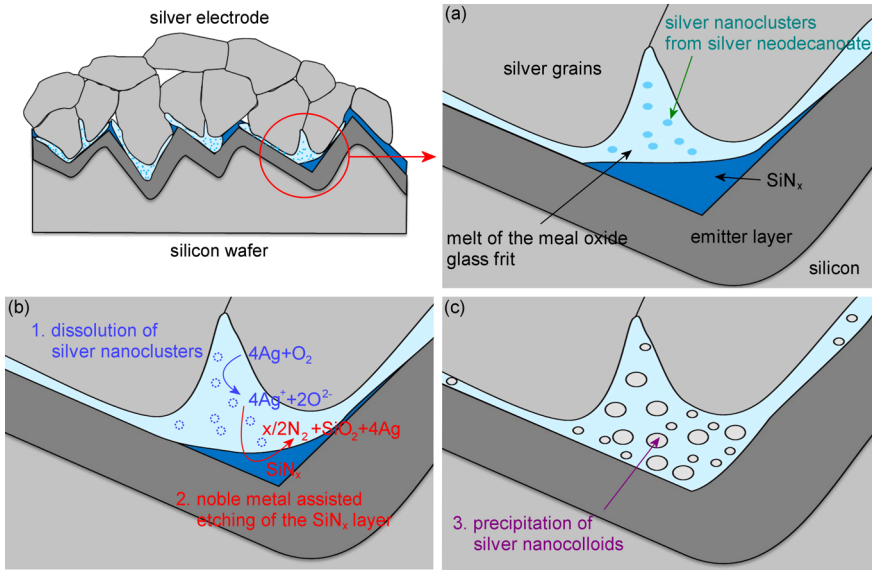


**Figure 9.** Illustration of the contact resistivity decreasing mechanism: (a) formation of silver nanoclusters, followed by the melting of metal oxide glass frit; (b) dissolution of silver nanoclusters in the melt of metal oxide glass frit and the subsequent noble-metal-assisted etching of $SiN_x$; and (c) precipitation of silver nanocolloids during the cooling stage.

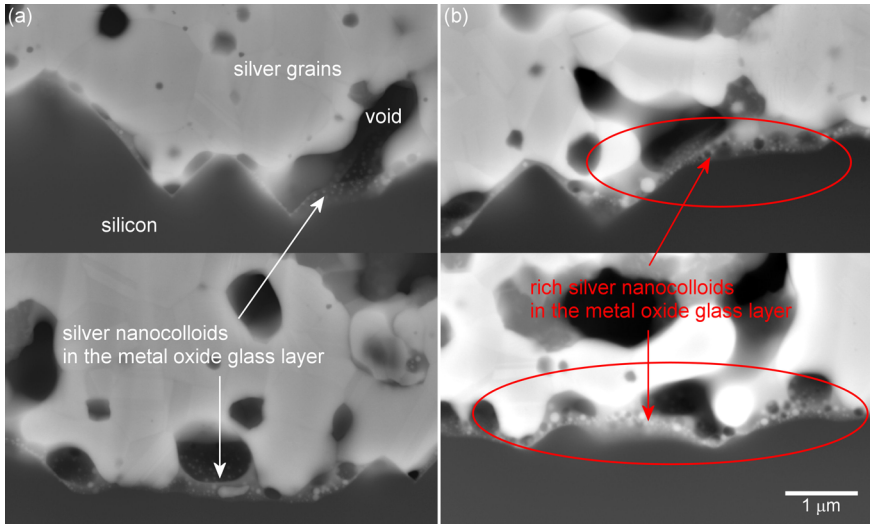


**Figure 10.** Comparison of the abundance of silver nanocolloids in the solidified metal oxide glass layer at a low peak firing temperature: silver paste (a) without and (b) with silver neodecanoate.

solar cells, it could provide a good method to ensure low contact resistivity over the broad range of peak firing temperatures required by silicon solar cell applications.

## AUTHOR INFORMATION

### Corresponding Authors

*E-mail: dongyoun.shin@gmail.com (D.-Y.S.).
*E-mail: mgkang@kier.re.kr (M.G.K.).

### Notes

The authors declare no competing financial interest.

## ACKNOWLEDGMENTS

This work was supported by the Basic Science Research Program through the National Research Foundation of Korea (NRF), which is funded by the Ministry of Education, Science and Technology (No. 2012R1A1A2038889) and the Research and Development Program of the Korea Institute of Energy Research (KIER) (B4-2422).

## REFERENCES

(1) Swanson, R. M. A Vision for Crystalline Silicon Photovoltaics. *Prog. Photovoltaics* **2006**, *14*, 443−453.
(2) Powell, D. M.; Winkler, M. T.; Choi, H. J.; Simmons, C. B.; Berney Needleman, D.; Buonassisi, T. Crystalline Silicon Photovoltaics: a Cost Analysis Framework for Determining Technology Pathways to Reach Baseload Electricity Costs. *Energy Environ. Sci.* **2012**, *5*, 5874−5883.
(3) Mette, A.; Richter, P. L.; Hörteis, M.; Glunz, S. W. Metal Aerosol Jet Printing for Solar Cell Metallization. *Prog. Photovoltaics* **2007**, *15*, 621−627.
(4) Hörteis, M.; Glunz, S. W. Fine Line Printed Silicon Solar Cells Exceeding 20% Efficiency. *Prog. Photovoltaics* **2008**, *16*, 555−560.
(5) Pospischil, M.; Zengerle, K.; Specht, J.; Birkle, G.; Koltay, P.; Zengerle, R.; Henning, A.; Neidert, M.; Mohr, C.; Clement, F.; Biro, D. Investigations of Thick-Film-Paste Rheology for Dispensing Applications. *Energy Procedia* **2011**, *8*, 449−454.
(6) Gizachew, Y. T.; Escoubas, L.; Simon, J. J.; Pasquinelli, M.; Loiret, J.; Leguen, P. Y.; Jimeno, J. C.; Martin, J.; Apraiz, A.; Aguerre, J. P. Towards Ink-Jet Printed Fine Line Front Side Metallization of Crystalline Silicon Solar Cells. *Sol. Energy Mater. Sol. Cells* **2011**, *95*, S70−S82.
(7) Shin, D.-Y.; Cha, Y.-K.; Ryu, H.-H.; Kim, S.-H. Impact of Effective Volume Ratio of a Dispersant to Silver Nano-Particles on Silicon Solar Cell Efficiency in Direct Ink-Jet Metallization. *J. Micromech. Microeng.* **2012**, *22*, 115007.
(8) Jang, Y.; Tambunan, I. H.; Tak, H.; Nguyen, V. D.; Kang, T.; Byun, D. Non-Contact Printing of High Aspect Ratio Ag Electrodes for Polycrystalline Silicone Solar Cell with Electrohydrodynamic Jet Printing. *Appl. Phys. Lett.* **2013**, *102*, 123901.
(9) Pysch, D.; Mette, A.; Filipovic, A.; Glunz, S. W. Comprehensive Analysis of Advanced Solar Cell Contacts Consisting of Printed Fine-line Seed layers Thickened by Silver Plating. *Prog. Photovoltaics* **2009**, *17*, 101−114.
(10) Lee, E. J.; Kim, D. S.; Lee, S. H. Ni/Cu Metallization for Low-Cost High-Efficiency PERC Cells. *Sol. Energy Mater. Sol. Cells* **2002**, *74*, 65−70.
(11) Chaudhari, V. A.; Solanki, C. S. A Novel Two Step Metallization of Ni/Cu for Low Concentrator c-Si Solar Cells. *Sol. Energy Mater. Sol. Cells* **2010**, *94*, 2094−2101.
(12) Foggiato, J.; Yoo, W. S.; Ouaknine, M.; Murakami, T.; Fukada, T. Optimizing the Formation of Nickel Silicide. *Mater. Sci. Eng., B* **2004**, *114*−*115*, 56−60.
(13) Narasimha, S.; Rohatgi, A. An Optimized Rapid Aluminum Back Surface Field Technique for Silicon Solar Cells. *IEEE Trans. Electron Devices* **1999**, *46*, 1363−1370.
(14) Kim, S. J.; Kim, S. Y.; Park, J. M.; Park, K. H.; Lee, J. H.; Lee, S. M.; Han, I. T.; Kim, D. H.; Lim, K. R.; Kim, W. T.; Park, J. C.; Jee, S. S.; Lee, E.-S. Thermal Decomposition of Silver Acetate in Silver Paste for Solar Cell Metallization: An Effective Route to Reduce Contact Resistance. *Appl. Phys. Lett.* **2013**, *103*, 063903.
(15) Ionkin, A. S.; Fish, B. M.; Li, Z. R.; Liang, L.; Lewittes, M. E.; Cheng, L. K.; Westphal, C.; Pepin, J. G.; Gao, F. Quaternary Phosphonium Salts as Cationic Selective Dispersants in Silver Conductive Pastes for Photovoltaic Applications. *Sol. Energy Mater. Sol. Cells* **2014**, *124*, 39−47.
(16) Hörteis, M.; Gutberlet, T.; Reller, A.; Glunz, S. W. High-Temperature Contact Formation on n-Type Silicon: Basic Reactions and Contact Model for Seed-layer Contacts. *Adv. Funct. Mater.* **2010**, *20*, 476−484.
(17) Vinod, P. N.; Chakravarty, B. C.; Lal, M.; Kumar, R.; Singh, S. N. A Novel Method for the Determination of the Front Contact Resistance in Large Area Screen Printed Silicon Solar Cells. *Semicond. Sci. Technol.* **2000**, *15*, 286−290.
(18) Vinod, P. N. Specific Contact Resistance Measurements of the Screen-Printed Ag Thick Film Contacts in the Silicon Solar Cells by Three-Point Probe Methodology and TLM Method. *J. Mater. Sci.:Mater. Electron.* **2011**, *22*, 1248−1257.

(19) Vinod, P. N. The Electrical and Microstructural Properties of Electroplated Screen-Printed Ag Metal Contacts in Crystalline Silicon Solar Cells. *RSC Adv.* **2013**, *3*, 14106−14113.
(20) Dearden, A. L.; Smith, P. J.; Shin, D.-Y.; Reis, N.; Derby, B.; O'Brien, P. A Low Curing Temperature Silver Ink for Use in Ink-Jet Printing and Subsequent Production of Conductive Tracks. *Macromol. Rapid Commun.* **2005**, *26*, 315−318.
(21) Shin, D.-Y.; Jung, M.; Chun, S. Resistivity Transition Mechanism of Silver Salts in the Next Generation Conductive Ink for a Roll-To-Roll Printed Film with a Silver Network. *J. Mater. Chem.* **2012**, *22*, 11755−11764.
(22) Lu, C.-A.; Lin, P.; Lin, H.-C.; Wang, S.-F. Effects of Metallo-Organic Decomposition Agents on Thermal Decomposition and Electrical Conductivity of Low-Temperature-Curing Silver Paste. *Jpn. J. Appl. Phys.* **2006**, *45*, 6987−6992.
(23) Lu, C.-A.; Lin, P.; Lin, H.-C.; Wang, S.-F. Characterization of the Low-Curing-Temperature Silver Paste with Silver 2-Ethylhexanoate Addition. *Jpn. J. Appl. Phys.* **2007**, *46*, 251−255.
(24) Fiorucci, A. R.; Saran, L. M.; Cavalheiro, É. T. G.; Neves, E. A. Thermal Stability and Bonding in the Silver Complexes of Ethylenediaminetetraacetic Acid. *Thermochim. Acta* **2000**, *356*, 71−78.
(25) Yamamoto, M.; Kashiwagi, Y.; Nakamoto, M. Size-Controlled Synthesis of Monodispersed Silver Nanoparticles Capped by Long-Chain Alkyl Carboxylates from Silver Carboxylate and Tertiary Amine. *Langmuir* **2006**, *22*, 8581−8586.
(26) Yang, M. X.; Jacobs, P. W.; Yoon, C.; Muray, L.; Anderson, E.; Attwood, D.; Somorjai, G. A. Thermal Stability of Uniform Silver Clusters Prepared on Oxidized Silicon and Aluminum Surfaces by Electron Beam Lithography in Oxidizing and Reducing Ambients. *Catal. Lett.* **1997**, *45*, 5−13.
(27) Bokhonov, B.; Korchagin, M. In-Situ Investigation of the Formation of Eutectic Alloys in the Systems Silicon-Silver and Silicon-Copper. *J. Alloys Compd.* **2002**, *335*, 149−156.
(28) Logvinenko, V.; Polunina, O.; Mikhailov, Y.; Mikhailov, K.; Bokhonov, B. Study of Thermal Decomposition of Silver Acetate. *J. Therm. Anal. Calorim.* **2007**, *90*, 813−816.
(29) Cabrera, E.; Olibet, S.; Glatz-Reichenbach, J.; Kopecek, R.; Reinke, D.; Schubert, G. Experimental Evidence of Direct Contact Formation for the Current Transport in Silver Thick Film Metallized Silicon Emitters. *J. Appl. Phys.* **2011**, *110*, 114511.
(30) Hong, K.-K.; Cho, S.-B.; You, J. S.; Jeong, J.-W.; Bea, S.-M.; Huh, J.-Y. Mechanism for the Formation of Ag Crystallites in the Ag Thick-Film Contacts of Crystalline Si Solar Cells. *Sol. Energy Mater. Sol. Cells* **2009**, *93*, 898−904.
(31) Cho, S.-B.; Hong, K.-K.; Huh, J.-Y.; Park, H. J.; Jeong, J.-W. Role of the Ambient Oxygen on the Silver Thick-Film Contact Formation for Crystalline Silicon Solar Cells. *Curr. Appl. Phys.* **2010**, *10*, S222−S225.
(32) Huh, J.-Y.; Hong, K.-K.; Cho, S.-B.; Park, S.-K.; Lee, B.-C.; Okamoto, K. Effect of Oxygen Partial Pressure on Ag Crystallite Formation at Screen-Printed Pb-Free Ag Contacts of Si Solar Cells. *Mater. Chem. Phys.* **2011**, *131*, 113−119.
(33) Chung, B.-M.; Cho, S.-B.; Chun, J.-W.; Kim, Y.-S.; Okamoto, K.; Huh, J.-Y. Influence of Oxygen on Ag Ionization in Molten Lead Borosilicate Glass during Screen-Printed Ag Contact Formation for Si Solar Cells. *Electrochim. Acta* **2013**, *106*, 333−341.
(34) Huang, Z.; Geyer, N.; Werner, P.; de Boor, J.; Gösele, U. Metal-Assisted Chemical Etching of Silicon: A Review. *Adv. Mater.* **2011**, *23*, 285−308.
(35) Zhong, X.; Qu, Y.; Lin, Y.-C.; Liao, L.; Duan, X. Unveiling the Formation Pathway of Single Crystalline Porous Silicon Nanowires. *ACS Appl. Mater. Interfaces* **2011**, *3*, 261−270.
(36) Lianto, P.; Yu, S.; Wu, J.; Thompson, C. V.; Choi, W. K. Vertical Etching with Isolated Catalysis in Metal-Assisted Chemical Etching of Silicon. *Nanoscale* **2012**, *4*, 7532−7539.
(37) Li, X.; Xiao, Y.; Bang, J. H.; Lausch, D.; Meyer, S.; Miclea, P.-T.; Jung, J.-Y.; Schweizer, S. L.; Lee, J.-H.; Wehrspohn, R. B. Upgraded Silicon Nanowires by Metal-Assisted Etching of Metallurgical Silicon: A New Route to Nanostructured Solar-Grade Silicon. *Adv. Mater.* **2013**, *25*, 3187−3191.
(38) Li, L.; Liu, Y.; Zhao, X.; Lin, Z.; Wong, C.-P. Uniform Vertical Trench Etching on Silicon with High Aspect Ratio by Metal-Assisted Chemical Etching Using Nanoporous Catalysts. *ACS Appl. Mater. Interfaces* **2014**, *6*, 575−584.
(39) Li, Z. G.; Liang, L.; Cheng, L. K. Electron Microscopy Study of Front-Side Ag Contact in Crystalline Si Solar Cells. *J. Appl. Phys.* **2009**, *105*, 066102.